AIAA JOURNAL
Vol. 45, No. 5, May 2007

Scalar Fluctuation Modeling for High-Speed Aeropropulsive Flows

Kevin W. Brinckman,* William H. Calhoon Jr.,† and Sanford M. Dash‡
Combustion Research and Flow Technology, Inc., Pipersville, Pennsylvania 18947

DOI: 10.2514/1.21075

A Reynolds-averaged Navier–Stokes-based scalar-variance model is described that extends a previous low-speed nonreacting jet model to more generalized high-speed compressible reacting flows. The model is cast in a k–ε turbulence model framework. Transport equations for energy variance and its dissipation rate are solved to predict temperature fluctuations and provide a thermal time scale for use in calculating a variable turbulent Prandtl number. For multispecies problems, mixture-fraction variance and dissipation rate equations are solved that predict species concentration fluctuations and provide a species mixing time scale for use in calculating a variable turbulent Schmidt number. The formulation accounts for compressibility and near-wall damping effects. A series of high-speed flow simulations are presented for both nonreacting and reacting configurations and the predictions are compared to available measured data and companion LES calculations. Results demonstrate the models' capabilities over a range of conditions and suggest that the proposed formulation will provide improved predictions in practical high-speed aeropropulsive configurations of interest, such as scramjet combustors, where turbulent Prandtl and Schmidt numbers vary substantially.

Nomenclature

C_v	=	specific heat
c	=	speed of sound
D	=	molecular species diffusion coefficient
D_t	=	turbulent species diffusion coefficient
e	=	specific internal energy
e''	=	fluctuating internal energy
f	=	mixture fraction
f_λ	=	scalar-variance damping function
f_μ	=	turbulence near-wall damping function
f''	=	fluctuating mixture fraction
k	=	turbulent kinetic energy
k_e	=	energy variance
k_f	=	mixture-faction variance
k_T	=	temperature variance
M_T	=	turbulent Mach number, $\sqrt{2k}/c$
P_k	=	turbulent kinetic energy production rate
$\hat{P}_k$	=	P_k with compressibility correction
Pr	=	molecular Prandtl number
Pr_t	=	turbulent Prandtl number
r_c	=	distance from jet centerline
Re_k	=	turbulent Reynolds number, $\rho\sqrt{k}y/\mu$
Re_t	=	turbulent Reynolds number, $k^2/\nu\varepsilon$
Sc	=	molecular Schmidt number
Sc_t	=	turbulent Schmidt number
T	=	static temperature
T_t	=	total temperature
u_j	=	mean velocity
u_ε	=	Kolmogorov velocity scale, $(\nu\varepsilon)^{1/4}$
y^*	=	sublayer scaled distance, $u_\varepsilon y/\nu$
y^+	=	sublayer scaled distance, $u_\tau y/\nu$
α	=	thermal diffusivity
α_t	=	turbulent thermal diffusivity
ε	=	turbulence dissipation rate
ε_e	=	energy-variance dissipation rate
ε_f	=	mixture-fraction variance dissipation rate
ε_T	=	temperature variance dissipation rate
μ	=	instantaneous fluid viscosity
μ_t	=	eddy viscosity
ν_t	=	kinematic eddy viscosity, μ_t/ρ
ρ	=	density
τ_m	=	turbulent scalar diffusion time scale
$\bar{}$	=	time-averaged quantity
$\tilde{}$	=	Favré-averaged quantity

Subscripts

e	=	energy variance
f	=	mixture-fraction variance
j	=	jet
T	=	temperature variance
w	=	wall
∞	=	freestream

Received 11 November 2005; accepted for publication 14 October 2006. Copyright © 2007 by the authors. Published by the American Institute of Aeronautics and Astronautics, Inc., with permission. Copies of this paper may be made for personal or internal use, on condition that the copier pay the $10.00 per-copy fee to the Copyright Clearance Center, Inc., 222 Rosewood Drive, Danvers, MA 01923; include the code 0001-1452/07 $10.00 in correspondence with the CCC.

*Research Scientist, 6210 Keller's Church Road. Member AIAA.
†Senior Research Scientist, 6210 Keller's Church Road. Member AIAA.
‡President and Principal Chief Scientist, 6210 Keller's Church Road. Associate Fellow AIAA.

I. Introduction

TURBULENT flows exhibit complex, nonlinear, unsteady, multiscale characteristics, which can have a large influence on heat and mass transfer. The simulation of high-speed aeropropulsive configurations, such as scramjet combustors, missile and rocket plumes, and fighter jet exhausts, must account for turbulent mixing to produce an accurate prediction of the flow. For example, missile/rocket base heating and pressure distribution predictions must account for turbulence effects in the structure of the base flow, plume temperature distribution, and entrainment of exhaust gases. Turbulent density fluctuation predictions in jet plumes are essential for reliable aerooptical assessments, and in a reacting environment, combustion performance is directly influenced by the turbulent mixing and distribution of the fuel/oxidizer species and temperature. Although models to capture turbulence effects on the velocity field have undergone substantial development in the past several decades, there has been less focus on refining turbulent mixing predictions of scalar quantities, such as species and temperature. The current work presents an extension of a Reynolds-averaged Navier–Stokes (RANS) formulation for predicting turbulent mixing of temperature in nonreacting compressible flows to a model for turbulent species

and energy transport, which can be applied over a range of flows from low-speed/low-temperature flows to high-speed reacting flows.

Turbulent energy and species transport, in high-speed aeropropulsive flows, are known to occur at different rates than turbulent momentum transport. Most often, these rates are faster, and in traditional RANS simulations this difference is accounted for using turbulent Prandtl Pr_t and Schmidt Sc_t numbers in the diffusion coefficient for the energy and species transport equations. Using a gradient transport hypothesis, turbulent diffusivity is related to the turbulent eddy viscosity by the relation

$$\alpha_t = \frac{\nu_t}{Pr_t} \tag{1}$$

In the case of species diffusion, a turbulent mass diffusivity D_t is calculated using Sc_t, as the characteristic quantity

$$D_t = \frac{\nu_t}{Sc_t} \tag{2}$$

Use of single (constant) values of Pr_t and Sc_t may suffice for simple flows (i.e., $Pr_t = 0.6$–0.7 in a fully developed, hot round jet), but for more complex aeropropulsive flows (such as scramjet fuel injection flowfields or divert jets on a hypersonic missile), these values can vary substantially in both time and space. The practical remedy has been to calculate local values of Pr_t and Sc_t, based on time-scale relations, by solving scalar variance and dissipation rate equations, having the same general form as the k–ε turbulence model equations. The current work considers such an approach, extending the model of Sommer et al. [1] for temperature variance in nonreacting flows, to an energy-variance formulation for Pr_t and a mixture-fraction variance formulation for Sc_t, which can be used in both nonreacting and reacting aeropropulsive flows for improved scalar mixing predictions [2,3].

A two-equation scalar-variance model coupled to a k–ε turbulence model is used to predict local values of turbulent scalar diffusivity, which is equivalent to using a variable turbulent Prandtl number in Eq. (1). Earlier two-equation models for turbulent heat transfer in wall-bounded flows by Nagano and Kim [4], Nagano et al. [5], and Sommer et al. [6] provided a turbulent Prandtl number formulation for incompressible flows. The Sommer et al. [6] model was based on the variance equations provided by Launder [7]. Sommer et al. [1] extended the model to consider high-speed compressible turbulent boundary layers adopting the approach of Zhang et al. [8] for a near-wall compressible k–ε formulation. The current scalar-variance model is based on the temperature variance method for variable Prandtl number of Sommer et al. [1] for high-speed compressible flows. The k–ε turbulence model implemented by the authors adopts features of the Zhang et al. [8] formulation for near-wall compressible flows and has consistency with the Sommer et al. [1] approach for scalar-variance modeling. Details of the turbulence models are provided in a later section.

The approach used by Sommer et al. [1] to derive a variable turbulent Prandtl number considers a time scale for turbulent heat transfer τ_m, which is based on the turbulent velocity and thermal time scales

$$\tau_m = \sqrt{\frac{k}{\varepsilon}\frac{k_T}{\varepsilon_T}} \tag{3}$$

The current model generalizes the temperature variance formulation of Sommer et al. [1] to allow for modeling of high-speed reacting jet and plume flows by solving for internal energy variance, which is relevant to multispecies flows with nonuniform gas properties. In addition, this approach allows modeling of chemically reacting problems without introducing chemical source terms in the variance equation, which are problematic [9]. The energy variance $k_e = \widetilde{e''e''}$ and its dissipation rate ε_e can be used in place of the temperature variance and dissipation rate to derive the thermal time scale in Eq. (3). Similarly, a mixture-fraction variance $k_f = \widetilde{f''f''}$ model is derived, where f is the mixture fraction in a two-stream problem, to provide a relation for the time scale of species fluctuations in calculation of a turbulent Schmidt number and mass diffusivity.

Prior work by one of the authors [10] presented a model for temperature variance and turbulent Prandtl number, which was shown to perform well for subsonic jets in capturing both the mean and fluctuating temperature field as compared to measured data. At supersonic and hypersonic flow speeds, compressibility effects must be accounted for in calculating both mean and turbulent quantities, and can have a significant effect on the fluctuation magnitude and time scale, and turbulent mixing. For example, temperature fluctuation predictions using large eddy simulation (LES) in both a low- and high-speed shear layer with the same temperature and velocity ratios were compared [11], with the fluctuations being lower for the high-speed case (as is turbulent kinetic energy). The current scalar-variance model is coupled to a compressibility-corrected k–ε turbulence model shown to adequately predict both low- and high-speed mixing flows [12] and capture the compressibility effects observed in the LES shear layer calculations, as will be described.

A recent survey article by Nagano [13] reviews a number of approaches proposed for modeling temperature variance in wall-bounded flows. Predictions from these models have been compared to basic nonreacting mixing problems; however, the models may not be well suited to reacting flows due to difficulties with the modeling of chemical source terms in the temperature variance formulation. The work of Xiao et al. [14] presents a formulation for predicting a variable turbulent Schmidt number in high-speed flows, using an equation for the sum of the variances of species mass fractions and its dissipation rate, and presents comparisons to nonreacting data sets. In a mass-fraction formulation, chemical source terms are again present in reacting flows, and some treatment of these terms must be applied. Xiao et al. [15] discuss problems encountered with modeling chemical source terms in scalar-variance models, and demonstrate the poor performance of their models when the chemical source terms are ignored. Improved comparisons to reacting data sets are realized when the chemical source terms are modeled. The scalar-variance models presented in the current paper avoid appearance of the chemical source terms altogether and should be better posed for application to problems in combustion.

The governing equations for both the energy-variance and mixture-fraction variance models are presented in the following section. Several validation studies are presented with comparison to data, for both reacting and nonreacting flows, which show that the energy and mixture-fraction variance approach can provide a significant improvement in the modeling of turbulent mixing effects. Results demonstrate that the predicted turbulent Prandtl and Schmidt numbers deviate from substantially uniform values across a flowfield when velocity and scalar gradients are present, indicating the need to use scalar-variance models for capturing the differences in turbulent thermal, species, and momentum transport.

II. Governing Equations

The compressible Navier–Stokes equations for mean density, velocity, and energy and the k–ε model for turbulent kinetic energy and dissipation rate are solved using a Roe-based finite volume scheme with Favré averaging. Additional equations for scalar variance and dissipation rate are directly coupled into the equation set; k_e–ε_e equations are included for internal energy variance, and k_f–ε_f equations are included for species mixture fraction.

A. Turbulent Kinetic Energy and Dissipation Rate Equations

The k–ε turbulence model is based on the original model for free-shear flows of Launder et al. [16] with enhancements incorporated to account for compressibility effects following the concepts of Sarkar [17] and Zeman [18], and round-jet vortex stretching following Pope [19] (whose use is restricted to concentric jets). The near-wall damping formulation of So et al. [20] is applied with modifications that permit usage of the original Launder et al. [16] coefficients in place of those of So et al. [20]. The k–ε model has the form

Table 1 k–ε model constants

Constant	Value
C_μ	0.09
$C_{\varepsilon 1}$	1.43
$C_{\varepsilon 2}$	1.92
$C_{\varepsilon 3}$	0.79
σ_k	1.0
σ_ε	1.3
α_1	2.5
α_2	2.0
β	75
λ	0.2

$$\frac{\partial \bar{\rho} k}{\partial t} + \frac{\partial \bar{\rho} \tilde{u}_j k}{\partial x_j} = \frac{\partial}{\partial x_j}\left[\left(\mu + \frac{\mu_t}{\sigma_k}\right)\frac{\partial k}{\partial x_j}\right] + P_k - \bar{\rho}\varepsilon + SS_k \tag{4}$$

$$\frac{\partial \bar{\rho} \varepsilon}{\partial t} + \frac{\partial \bar{\rho} \tilde{u}_j \varepsilon}{\partial x_j} = \frac{\partial}{\partial x_j}\left[\left(\mu + \frac{\mu_t}{\sigma_\varepsilon}\right)\frac{\partial \varepsilon}{\partial x_j}\right] + f_1 C_{\varepsilon 1} P_k \frac{\varepsilon}{k} - f_2 C_{\varepsilon 2} \bar{\rho} \hat{\varepsilon} \frac{\varepsilon}{k} + SS_\varepsilon \tag{5}$$

where

$$P_k = \bar{\rho} \tau_{ij} \frac{\partial \tilde{u}_i}{\partial x_j} \tag{6}$$

$$\mu_t = f_\mu C_\mu \bar{\rho} \frac{k^2}{\varepsilon} \tag{7}$$

$$\bar{\rho}\tau_{ij} = \mu_t\left(\frac{\partial \tilde{u}_i}{\partial x_j} + \frac{\partial \tilde{u}_j}{\partial x_i}\right) - \frac{2}{3}\delta_{ij}\left(\mu_t \frac{\partial \tilde{u}_n}{\partial x_n} + \bar{\rho} k\right) \tag{8}$$

Model constants are defined in Table 1. The functional coefficients $f_1 = 1 - e^{-(Re_t/40)^2}$, $f_2 = 1 - \frac{2}{9} e^{-(Re_t/6)^2}$, and f_μ, as well as the modified dissipation rate term $\hat{\varepsilon} = \varepsilon - \frac{14}{9}\frac{\mu}{\rho f_2}\frac{\partial \sqrt{k}}{\partial x_i}\frac{\partial \sqrt{k}}{\partial x_i}$, are related to the near-wall damping model of So et al. [20]. The compressibility correction used [12] is given by

$$SS_k = -\alpha_1 \hat{M}_T^2 P_k - \alpha_2 \hat{M}_T^2 \bar{\rho}\varepsilon \tag{9}$$

where $\hat{M}_T$ is lagged by a value of $\lambda = 0.2$, so that compressibility corrections do not initiate until this fluctuation level is exceeded. Thus,

$$\hat{M}_T = \max[M_T - \lambda, 0] \tag{10}$$

For round jets, in axisymmetric configurations, the vortex stretching correction of Pope [19], modified for compressibility is given by:

$$SS_\varepsilon = \exp(-\beta \hat{M}_T^2) C_{\varepsilon 3}\left[\frac{1}{4}\left(\frac{k}{\varepsilon}\right)^3 \left(\frac{\partial \tilde{u}_x}{\partial r} - \frac{\partial \tilde{u}_r}{\partial x}\right)^2 \frac{\tilde{u}_r}{r_c}\right]\bar{\rho}\frac{\varepsilon^2}{k} \tag{11}$$

This correction is applied to axisymmetric configurations with Eqs. (4) and (5) and cast in cylindrical coordinates, with x as the axial coordinate.

An important feature of the near-wall treatment is that it avoids use of boundary-layer-specific wall distance terms, such as y^+ and μ_τ, allowing for application of the model to more complex flows. The expression used for f_μ is

$$f_\mu = \left(1 + 4/Re_t^{3/4}\right)\tanh(Re_k/125) \tag{12}$$

Complete details of the k–ε model can be found in [12].

B. Internal Energy Variance and Dissipation Rate Equations

A transport equation for internal energy variance $k_e = \widetilde{e''e''}$ is derived by taking moments of the energy conservation equation with Favré averaging ($e = \tilde{e} + e''$) and employing the gradient diffusion hypothesis to model higher-order correlations. An equation for energy k_e variance and its dissipation rate ε_e coupled to the k–ε equations is formulated in analogy to that of Sommer et al. [1] for the temperature variance dissipation rate, including a near-wall treatment.

The transport equations for k_e and ε_e are given as

$$\frac{\partial(\bar{\rho}k_e)}{\partial t} + \frac{\partial(\bar{\rho}\tilde{u}_j k_e)}{\partial x_j} = \frac{\partial}{\partial x_j}\left[\bar{\rho}\left(\alpha + \frac{\alpha_t}{\sigma_{k,e}}\right)\frac{\partial k_e}{\partial x_j}\right] + 2\bar{\rho}\alpha_t\left(\frac{\partial \tilde{e}}{\partial x_j}\right)^2 - 2\bar{\rho}\varepsilon_e \tag{13}$$

$$\frac{\partial(\bar{\rho}\varepsilon_e)}{\partial t} + \frac{\partial(\bar{\rho}\tilde{u}_j \varepsilon_e)}{\partial x_j} = \frac{\partial}{\partial x_j}\left[\bar{\rho}\left(\alpha + \frac{\alpha_t}{\sigma_{\varepsilon,e}}\right)\frac{\partial \varepsilon_e}{\partial x_j}\right] + \bar{\rho}\alpha_t\left(C_{d1}\frac{\varepsilon_e}{k_e} + C_{d2}\frac{\varepsilon}{k}\right)\left(\frac{\partial \tilde{e}}{\partial x_j}\right)^2 + C_{d3}\hat{P}_k\frac{\varepsilon_e}{k} - \left(C_{d4}\frac{\varepsilon_e}{k_e} + C_{d5}\frac{\varepsilon}{k}\right)\bar{\rho}\varepsilon_e + \xi_{\varepsilon T} \tag{14}$$

where the dissipation rate is defined as

$$\bar{\rho}\varepsilon_e = \overline{\rho\alpha\frac{\partial e''}{\partial x_k}\frac{\partial e''}{\partial x_k}} \tag{15}$$

and the heat transfer time scale based on Eq. (3) is

$$\tau_{m,e} = \sqrt{\frac{k}{\varepsilon}\frac{k_e}{\varepsilon_e}} \tag{16}$$

The compressibility correction used in the k–ε model is carried over with the expression

$$\hat{P}_k = P_k - \alpha_1 \hat{M}_T^2 P_k - \alpha_2 \hat{M}_T^2 \bar{\rho}\varepsilon \tag{17}$$

$\xi_{\varepsilon T}$ is a near-wall damping function included to capture low-Reynolds-number behavior, based on the formulation in Sommer et al. [1]

$$\xi_{\varepsilon T} = f_{\varepsilon T}\bar{\rho}\left[(C_{d4} - 4)\frac{\hat{\varepsilon}_e}{k_e}\varepsilon_e + C_{d5}\frac{\hat{\varepsilon}}{k}\varepsilon_e - \frac{(\varepsilon_e^*)^2}{k_e}\right] \tag{18}$$

where $f_{\varepsilon T} = e^{-(Re_t/80)^2}$ is a damping term, $\hat{\varepsilon}_e = \varepsilon_e - \alpha(\frac{\partial\sqrt{k_e}}{\partial y})^2$, $\hat{\varepsilon} = \varepsilon - 2\nu(\frac{\partial\sqrt{k}}{\partial y})^2$, and $\varepsilon_e^* = \varepsilon_e - \frac{\alpha k_e}{y^2}$.

Constants used in the k_e–ε_e model are summarized in Table 2 and are consistent with those proposed by Sommer et al. [1] for near-wall flows, with the exception of $\sigma_{k,\varepsilon}$ and $\sigma_{\varepsilon,e}$. The current investigation found that the Sommer et al. [1] recommended values of $\sigma_{k,T} = 0.75$ and $\sigma_{\varepsilon,T} = 1.45$ for near-wall temperature variance modeling

Table 2 Scalar-variance model constants

Constant	Value
C_{d1}	2.0
C_{d2}	0.0
C_{d3}	0.72
C_{d4}	2.2
C_{d5}	0.8
$C_{1\lambda}$	0.1
A^+	45
$\sigma_{k,e}$	1.0
$\sigma_{\varepsilon,e}$	1.0
$\sigma_{k,f}$	1.0
$\sigma_{\varepsilon,f}$	1.0

resulted in overly diffusive scalar-variance predictions for free-shear flows when compared with data. Consistent with Chidambaram et al. [10], in their investigation of temperature variance modeling for propulsive jets, we have found that values of $\sigma_{k,e} = 1.0$ and $\sigma_{\varepsilon,e} = 1.0$ provide a better match to scalar fluctuation data for free-shear flows, while maintaining results for near-wall predictions comparable to those obtained with the Sommer et al. [1] recommended values.

The turbulent thermal diffusivity is calculated from

$$\alpha_t = C_\lambda f_\lambda k \tau_{m,e} \tag{19}$$

and the turbulent Prandtl number with near-wall damping is derived as

$$Pr_t = \frac{C_\mu f_\mu}{C_\lambda f_\lambda} \sqrt{\frac{k}{\varepsilon}\frac{\varepsilon_e}{k_e}} \tag{20}$$

where $C_\lambda = 0.14$, which differs slightly from the value presented by Sommer et al. [1] to better simulate the turbulent Prandtl number for axisymmetric jets.

To recover the asymptotic behavior of the turbulent heat flux near the wall, Sommer et al. [1] propose the use of the near-wall damping function f_λ, given by

$$f_\lambda = f_{\varepsilon T}\frac{C_{1\lambda}}{Re_t^{1/4}} + (1 - e^{-y^+/A^+})^2 \tag{21}$$

The relation of f_λ to y^+ in Eq. (21) presents problems when applying the k_e–ε_e model to complex flows where flow separation occurs and standard boundary layer relations may not be applicable. Abe and Kondoh [21] provide an alternative to the use of y^+, by employing the Kolmogorov velocity scale $u_\varepsilon = (\nu\varepsilon)^{1/4}$ to define a wall distance $y^* = u_\varepsilon y/\nu$, which can be applied in both attached and detached flows. We have found that the use of y^* in Eq. (21) yields similar near-wall damping behavior in attached flows and is well-behaved in separated flows. Thus, the expression for the near-wall damping function f_λ used in the current fluctuating-scalar model is

$$f_\lambda = f_{\varepsilon T}\frac{C_{1\lambda}}{Re_t^{1/4}} + (1 - e^{-y^*/A^+})^2 \tag{22}$$

The energy variance k_e and its dissipation rate ε_e go to zero at the freestream. At a wall, k_e goes to zero and ε_e behaves as $\varepsilon_e = \alpha_w(\partial\sqrt{k_e}/\partial y)_w^2$. For single species, constant-specific heat fluids, the k_e–ε_e formulation reduces exactly to the k_T–ε_T model of Brinckman et al. [22].

C. Mixture-Fraction Variance and Dissipation Rate Equations

A mixture-fraction variance formulation is developed to model the effects of species fluctuations on turbulent mass diffusivity and to provide inputs to turbulent combustion models. A Favré-averaged equation for mixture fraction ($f = \tilde{f} + f''$) mimics the species conservation equation, without the presence of a chemical source term, and is given by

$$\frac{\partial(\bar{\rho}\tilde{f})}{\partial t} + \frac{\partial(\bar{\rho}\tilde{u}_j\tilde{f})}{\partial x_j} = \frac{\partial}{\partial x_j}\left[\bar{\rho}(D + D_t)\frac{\partial\tilde{f}}{\partial x_j}\right] \tag{23}$$

where D is the molecular diffusion coefficient calculated from the local gas viscosity and Schmidt number, and D_t is the turbulent species diffusion coefficient. The mixture fraction behaves as a dilution ratio and represents the mass fraction of all the atoms originating from a given inlet (typically the fuel stream). Thus, f takes on a value of 1 at the tracked inlet and 0 at all other incoming boundaries. It is advantageous to work with a mixture fraction in reacting flows to avoid the appearance of chemical source terms in the equation used to predict species variance. The advantage arises in the fact that a mixture fraction itself is a conserved scalar, thus chemical source terms do not result on the right-hand side of the mixture-fraction equation and its corresponding variance equation in reacting flow problems. Alternative methods have been used to model species fluctuations based on mass fraction. In reacting flows, the mass-fraction-based species variance equation contains chemical source terms as higher-order moments of the species mass-fraction fluctuation and chemical reaction rate. These higher-order terms have proven difficult to accurately model and need to be neglected to avoid introducing additional error into the solution [9]. To avoid problems with chemical source terms in reacting problems, the mixture-fraction approach is used to predict species concentration variance and turbulent Schmidt number. Transport equations for the mixture-fraction variance $k_f = \widetilde{f''f''}$ and its dissipation rate ε_f are solved, coupled to the k–ε turbulence model. The transport equations for k_f and ε_f are similar to those for the energy variance and given as

$$\frac{\partial(\bar{\rho}k_f)}{\partial t} + \frac{\partial(\bar{\rho}\tilde{u}_j k_f)}{\partial x_j} = \frac{\partial}{\partial x_j}\left[\bar{\rho}\left(D + \frac{D_t}{\sigma_{k,f}}\right)\frac{\partial k_f}{\partial x_j}\right] + 2\bar{\rho}D_t\left(\frac{\partial\tilde{f}}{\partial x_j}\right)^2 - 2\bar{\rho}\varepsilon_f \tag{24}$$

$$\frac{\partial(\bar{\rho}\varepsilon_f)}{\partial t} + \frac{\partial(\bar{\rho}\tilde{u}_j\varepsilon_f)}{\partial x_j} = \frac{\partial}{\partial x_j}\left[\bar{\rho}\left(D + \frac{D_t}{\sigma_{\varepsilon,f}}\right)\frac{\partial\varepsilon_f}{\partial x_j}\right] + \bar{\rho}D_t\left(C_{d1}\frac{\varepsilon_f}{k_f} + C_{d2}\frac{\varepsilon}{k}\right)\left(\frac{\partial\tilde{f}}{\partial x_j}\right)^2 + C_{d3}\hat{P}_k\frac{\varepsilon_f}{k} - \left(C_{d4}\frac{\varepsilon_f}{k_f} + C_{d5}\frac{\varepsilon}{k}\right)\bar{\rho}\varepsilon_f + \xi_{\varepsilon f} \tag{25}$$

Here, the dissipation rate is defined as

$$\bar{\rho}\varepsilon_f = \overline{\rho D\frac{\partial f''}{\partial x_k}\frac{\partial f''}{\partial x_k}} \tag{26}$$

and the mass transfer time scale based on Eq. (3) is

$$\tau_{m,f} = \sqrt{\frac{k}{\varepsilon}\frac{k_f}{\varepsilon_f}} \tag{27}$$

The turbulent species diffusion coefficient is calculated from

$$D_t = C_\lambda f_\lambda k \tau_{m,f} \tag{28}$$

and the turbulent Schmidt number with near-wall damping is

$$Sc_t = \frac{C_\mu f_\mu}{C_\lambda f_\lambda}\sqrt{\frac{k}{\varepsilon}\frac{\varepsilon_f}{k_f}} \tag{29}$$

The scalar-variance damping term f_λ is that given by Eq. (22), and model constants are identical to those of the energy-variance model in Table 2. The near-wall damping terms $\xi_{\varepsilon f}$ is analogous to that used in the energy-variance model,

$$\xi_{\varepsilon f} = f_{\varepsilon T}\bar{\rho}\left[(C_{d4} - 4)\frac{\hat{\varepsilon}_f}{k_f}\varepsilon_f + C_{d5}\frac{\hat{\varepsilon}}{k}\varepsilon_f - \frac{(\varepsilon_f^*)^2}{k_f}\right] \tag{30}$$

where $\hat{\varepsilon}_f = \varepsilon_f - D(\frac{\partial\sqrt{k_f}}{\partial y})^2$ and $\varepsilon_f^* = \varepsilon_f - D\frac{k_f}{y^2}$. The mixture-fraction variance k_f and its dissipation rate ε_f go to zero at the freestream. At a wall, k_f goes to zero and ε_f behaves as $\varepsilon_f = D_w(\partial\sqrt{k_f}/\partial y)_w^2$.

In nonreacting problems, the mass fraction of an individual species behaves as a conserved scalar, and a mixture fraction can be derived by normalizing one of the species mass fractions. This approach provides computational efficiency by eliminating the need to solve an additional transport equation for mixture fraction. In reacting problems, the same approach can be used with an inert species, as its mass must be conserved. In the absence of an inert species, the additional equation for the mixture fraction itself must be solved to assure that the variance k_f is based on a conserved scalar.

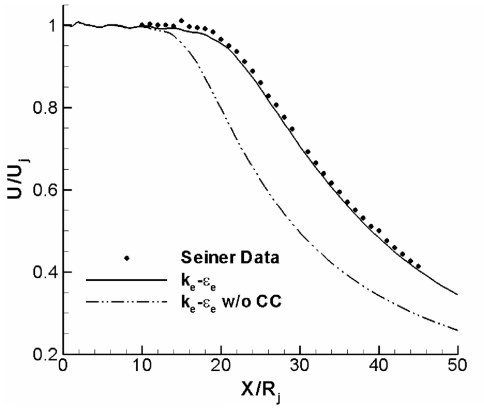

a) Centerline velocity

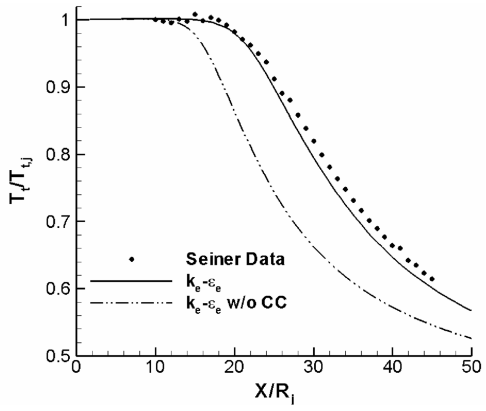

b) Centerline total temperature

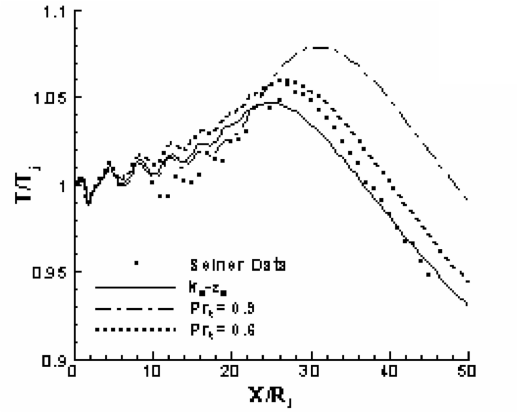

c) Centerline static temperature

Fig. 1 Mach 2 round jet predictions vs Seiner et al. [24] data.

III. Nonreacting Flow Studies: Energy Variance

A temperature variance model was previously used to predict temperature fluctuations in a low-speed Mach 0.24 axisymmetric nonreacting jet. Comparisons were made to centerline and radial, mean and fluctuating temperature data measured by Lockwood and Moneib [23]. The methodology and results provided by Chidambaram et al. [10] demonstrate that the proposed form of scalar-variance model performs well for subsonic axisymmetric flows. The current work extends that of Chidambaram et al. [10] to high-speed supersonic flows for both reacting and nonreacting conditions. Before considering more complex flows, several basic high-speed data sets were evaluated to assure that compressibility effects were properly accounted for with the scalar-variance model. In all cases, grid refinement studies were performed to assure that the results presented are grid-converged.

It is significant that in all cases presented in the current paper, the model formulation and constants outlined in the preceding section were used, without any case-specific refinement. Although some minor adjustment of constants could have been made on a case-by-case basis to improve comparisons, it is recognized that there is uncertainty in the measured data as well as in the calculations due to modeling simplifications and truncation error, and an "exact" match to all of the data sets is not anticipated. Instead, our intent in the data comparisons is to assess the capability of the proposed methodology to capture the flow physics for a range of high-speed aeropropulsive configurations without case-specific model tuning.

A. Mach 2.0 Hot Jet

First, we consider the hot, Mach 2 jet experiment of Seiner et al. [24] discharging into still air. The jet total temperature is 755.4 K and the surrounding ambient temperature is 300 K. This configuration was previously evaluated using a temperature variance model. Results reported by Brinckman et al. [22] for both a 755.4 and 1116.7 K jet compare favorably with experimental data and demonstrate that the temperature variance model is properly formulated for single-component, high-speed compressible jet flows with significant temperature gradients. Comparisons with data for the centerline velocity and total temperature variation using the current energy-variance model are provided in Figs. 1a and 1b. The calculated results with the compressibility correction of Eq. (17) agree well with the measured data and are identical to those from the temperature variance model [22], verifying that the energy and temperature variance models are consistent for a uniform composition, nonreacting flow, and that compressibility effects are properly accounted for in high-speed flows. The curve labeled "k_e–ε_e w/o CC" is the prediction without use of the compressibility correction in the turbulence model; the deviation from the measured data demonstrates the need for proper modeling to capture high-speed effects. Comparison of model predictions to static temperature data is provided in Fig. 1c, along with solutions produced using constant turbulent Prandtl numbers of 0.6 and 0.9. Here the energy-variance model acts to vary the turbulent Prandtl number throughout the domain and captures aspects of higher Prandtl number behavior in the potential core region and lower Prandtl number behavior downstream.

B. High-Speed Shear Layer: Uniform Gas Composition

The Mach 2 jet comparison demonstrates the capability of the energy-variance model to accurately predict mean temperatures at high-speed conditions. Because temperature fluctuation data at high speeds are scarce, 3-D LES studies were used to provide data on the fluctuating velocity and temperature field in free-shear layers. Calhoon et al. [11] performed LES studies on a supersonic ($M_c = 1.3$) air/air free-shear layer with a 3.33:1 temperature ratio ($T_2/T_1 = 1000/300$ K) and 6.1:1 velocity ratio ($u_2/u_1 = 1531/250.6$ m/s). A compressible form of the algebraic Smagorinsky model [25] was used for subgrid modeling. Inlet conditions for the LES case were specified to model naturally developing free-shear

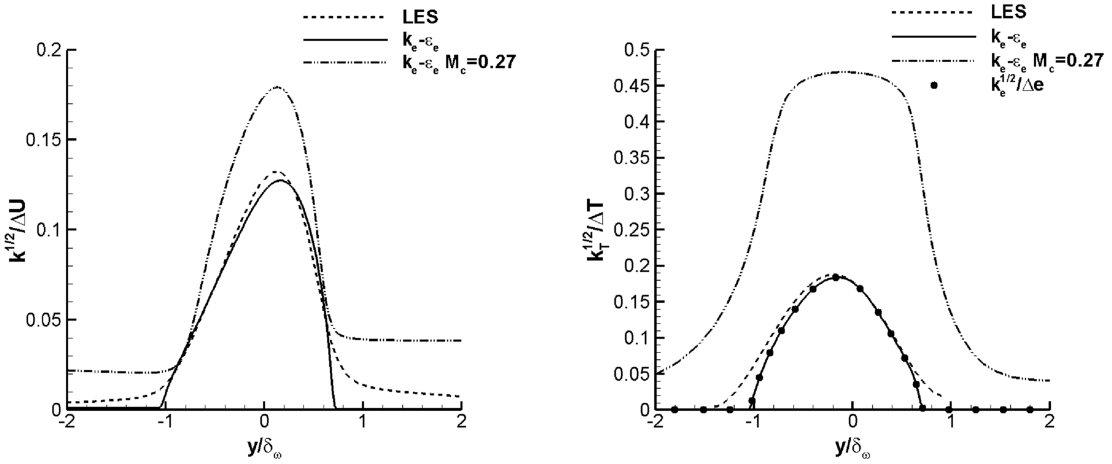

a) Turbulence intensity b) Temperature and energy fluctuation intensity

Fig. 2 High-speed air/air shear layer predictions with uniform specific heat.

flows. These boundary conditions are discussed in detail by Calhoon et al. [11], and were validated by comparison of predicted shear layer growth rate with experimental data. Numerically, the LES simulation used a fifth-order scheme for the inviscid fluxes, a fourth-order central scheme for the viscous and diffusive terms, and a fourth-order explicit time marching algorithm. The flowfield predicted by LES for the high-speed shear layer exhibits a large amount of fine-scale structure, in contrast to the large-scale spanwise rollers typical of a low-speed shear layer. The RANS turbulence boundary conditions considered background values of k, ε to mimic the LES inflow fluctuations. Sensitivity analyses showed that the background turbulence used in the RANS inflow boundary conditions produced little effect on the predicted turbulence and energy variance.

RMS data from the LES results was extracted for the fluctuating velocity and temperature fields to compare with the energy-variance model predictions. Figure 2 presents results of the current RANS k_e–ε_e simulations plotted in the self-similar region of the shear layer, where δ_ω is the vorticity thickness. Air is treated as an ideal gas with constant specific heat, and temperature variance is extracted from the predicted energy variance as $\widetilde{T''T''} = \widetilde{e''e''}/c_v^2$. Figure 2a shows the turbulence intensity, and Fig. 2b shows a comparison of the predicted temperature fluctuation intensity with respect to the temperature difference $\Delta T = T_2 - T_1$. Results from the RANS energy-variance model match the LES predictions for peak intensity for both velocity and temperature fluctuations within 5%. Although the agreement at the periphery of the shear region is not exact, the comparison is of primary interest at the high-gradient interface region, where the energy gradient in the source term of the energy-variance equation is the prominent mechanism in the evolution of the temperature fluctuations. Here, the test of the scalar-variance model is most critical, and the agreement with the LES data is good, without tuning of boundary conditions or model calibration constants.

The temperature variance from a k_T–ε_T solution presented by Brinckman et al. [22] is identical to that in Fig. 2b for the k_e–ε_e model. The internal energy fluctuation intensity $k_e^{1/2}/\Delta e$ is also plotted on the same scale. It is noted that the internal energy variance scales with the temperature variance for the uniform composition gas. Results of a low-speed ($M_c = 0.27$) shear layer RANS simulation with identical velocity and temperature ratios are included to illustrate the effects of compressibility on scalar fluctuations and mixing. The intensity levels in Fig. 2 are lower for the high-speed supersonic shear layer as compressibility tends to dampen the turbulent fluctuations. The average predicted turbulent Prandtl number for the low-speed shear layer is significantly lower than the average high-speed value of $Pr_t = 0.7$.

C. High-Speed Shear Layer: Variable Composition Gas

The previous air/air shear layer solutions demonstrate that the k_e–ε_e and k_T–ε_T models produce equivalent values for temperature variance in situations where the gas composition is uniform and variations in specific heat are neglected. The problem is repeated here with a temperature-dependent specific heat. Figure 3 plots predicted self-similar temperature fluctuation intensity from the k_e–ε_e model, compared to the LES data. Internal energy fluctuation intensity is plotted on the same scale. All compare closely with a slight deviation between the energy and temperature fluctuation intensity due to a small variation of specific heat with temperature. A second case considers an air/helium shear layer with the previous temperature and velocity ratios. The ratio of specific heat at freestream conditions is $c_{v,\text{air}}/c_{v,\text{he}} \approx 0.27$. Figure 4a presents the temperature fluctuation intensity for the air/helium shear layer predicted from both the k_e–ε_e and k_T–ε_T models. Here, we can see a deviation in the predicted temperature variance as the k_e–ε_e model considers the gradient in internal energy in the k_e source term and uses the local value of c_v to extract the temperature variance, whereas the k_T–ε_T model uses the temperature gradient for the k_T source term. It is interesting to compare the profiles for normalized mean temperature and internal energy (quantities are normalized with respect to the freestream) in Fig. 4b, which illustrates the appreciable difference in the gradients used in the production term for k_T vs k_e. Finally, an air–hydrogen shear layer is considered with the same temperature and velocity ratios, but a larger ratio of specific heats $c_{v,\text{air}}/c_{v,h2} \approx 0.084$. The temperature fluctuation intensity predicted by both models is presented in Fig. 5a. A more pronounced difference in both the magnitude and shape of the temperature variance resulted due to the significant variation in gas properties between air and hydrogen. Based on sensitivity studies, the temperature variance calculated from the energy variance as $\widetilde{T''T''} = \widetilde{e''e''}/c_v^2$ is expected to be within 10% of a more rigorous derivation with fluctuation intensities below

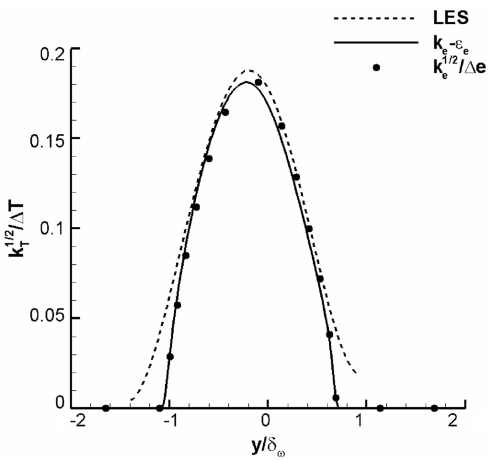

Fig. 3 High-speed air/air shear layer temperature and energy fluctuation intensity with variable specific heat.

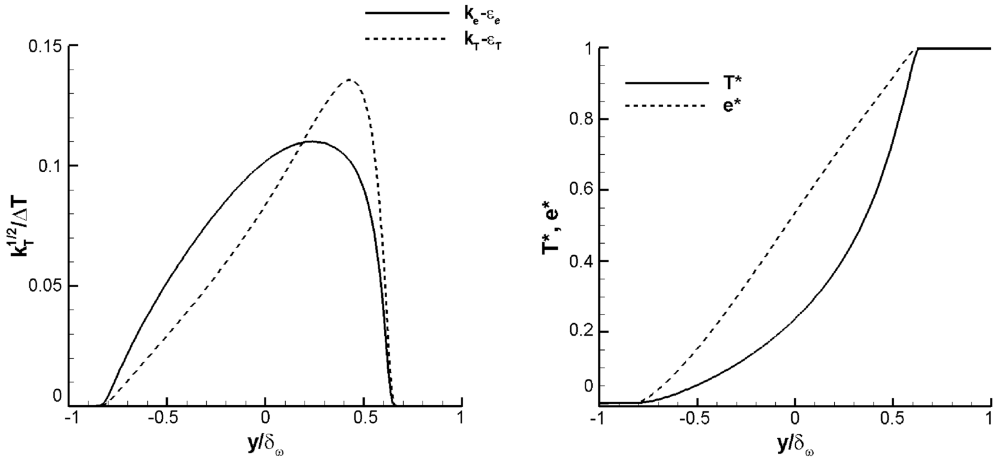

a) Temperature and energy fluctuation intensity b) Mean temperature and internal energy

Fig. 4 Air/helium shear layer.

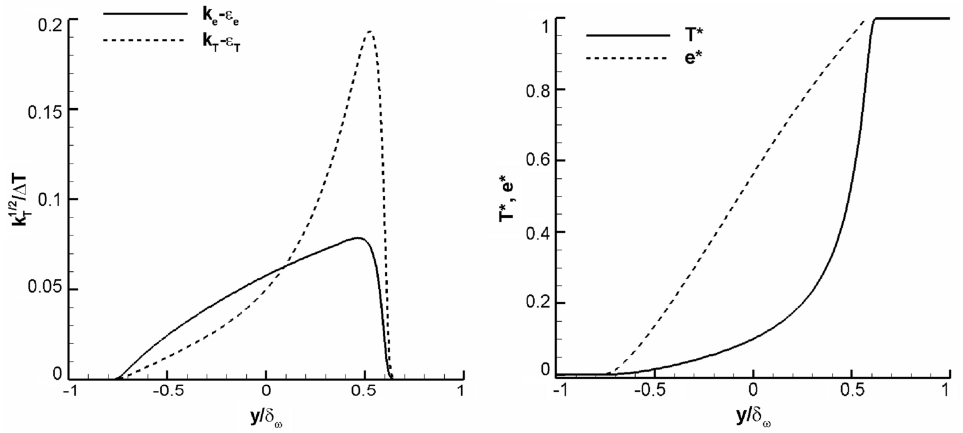

a) Temperature and energy fluctuation intensity b) Mean temperature and internal energy

Fig. 5 Air/hydrogen shear layer.

50%. Mean temperature and internal energy profiles in the self-similar region are presented for the air–hydrogen shear layer in Fig. 5b. As expected, the deviation between temperature and internal energy is greater than the air–helium shear layer because of the larger differences in gas specific heats.

The variable composition shear layer studies reveal the breakdown in the temperature variance k_T–ε_T model as nonuniform gas properties are encountered. The results suggest that in single-species applications, the k_T–ε_T model can be accurately applied to predict temperature variance $\widetilde{T''T''}$ as long as the gas specific heat is not overly sensitive to temperature variations. For situations with nonuniform gas properties throughout the flowfield, the k_T–ε_T model will become increasingly inaccurate and the energy-variance k_e–ε_e model is better suited to predict the temperature variance.

IV. Nonreacting Flow Studies: Species Variance

The mixture-fraction variance model equations, used to predict turbulent species mixing, are developed from the temperature variance model equations. Given the same turbulence field (k, ε),

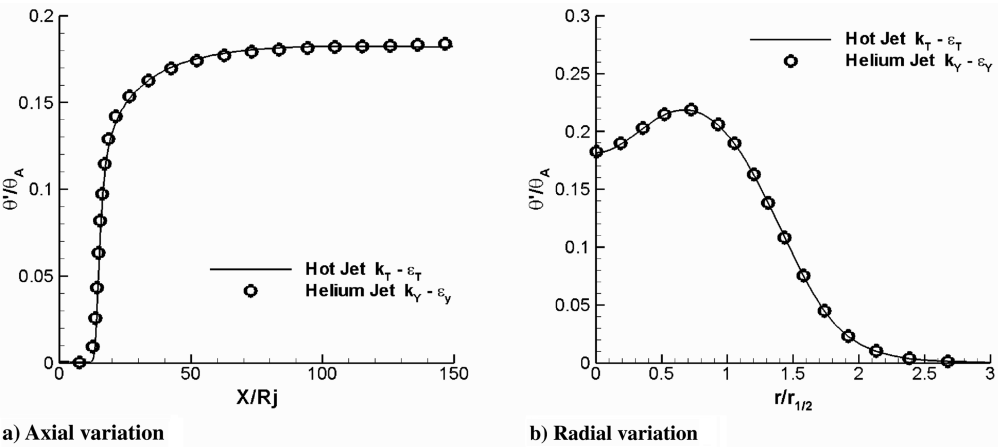

a) Axial variation b) Radial variation

Fig. 6 Mach 0.85 round-jet scalar fluctuation predictions for a hot jet vs helium jet.

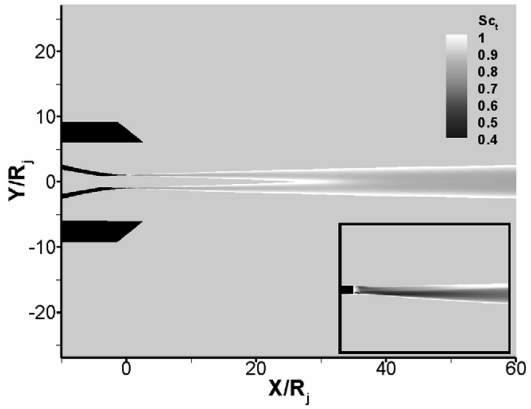

Fig. 7 Coflow helium–air jet contours of turbulent Schmidt number.

mean velocities, and density, the two models should provide the same scalar fluctuation levels for similar mean scalar gradients, in a nonreacting flow. Figure 6 shows a comparison of predicted fluctuations for two axial jets; one case considers temperature fluctuations for a hot jet of uniform composition discharging into a cold freestream, whereas the other considers species fluctuations for an isothermal helium jet discharging into an air freestream. The density ratio $\rho_{\text{jet}}/\rho_\infty$ is the same in both cases. The radial and centerline fluctuation intensity, that is, normalized variance, for both jets are identical, where θ_A refers to the difference between the Favré-averaged mean scalar value at the axis and freestream. θ' is the square root of the predicted variance and represents the magnitude of the fluctuation. This fundamental test case demonstrates that the predicted mixture-fraction variance evolves appropriately with the model equations and constants, as posed. We now consider several validation cases to determine whether the mixture-fraction variance model provides accurate prediction of turbulent species transport, in nonreacting flows.

A. Coflow Helium/Air Jet

A nonreacting, coflow jet is analyzed using the mixture-fraction variance k_f–ε_f model to predict turbulent mass diffusivity. Two uniform coaxial jets discharge at Mach 1.8 into still air. The center jet consists of 95% He and 5% O_2 by volume discharging from a 10-mm-diam nozzle. The outer air jet has a nozzle outer diameter of 60.47 mm. Both jets exit at atmospheric pressure. Two cases are considered; in one case, the mixture-fraction variance model is used to provide a variable turbulent Schmidt number and turbulent mass diffusivity, employing Eqs. (27–29). In a second case, a constant value for turbulent Schmidt number, $Sc_t = 0.7$, is used as typical of what may be considered reasonable for a round jet. Results for mean mass fraction and velocity are compared with the experimental data of Cutler et al. [26,27]. The nozzle geometry is modeled and grid refinement performed. Figure 7 shows contours of turbulent Schmidt number predicted with the proposed model, against a background freestream value of $Sc_t = 0.9$. A closeup of the inner-nozzle region shows the largest deviation from freestream occurs at the nozzle exit between the boundary of the two jet streams, where the value of Sc_t is at its minimum. The variation in Sc_t through the domain is an indication of the difference in turbulence and turbulent species diffusion time scales, as reflected in the definition of turbulent Schmidt number in Eq. (29). Figure 8 provides comparisons to experimental data [26,27] for velocity and mixing of the center jet species. Predicted velocities compare well to the measured data in Fig. 8a, allowing a relevant assessment of the species mixing model. The predicted helium–O_2 mass-fraction distribution is compared with experimental data in Fig. 8b. Results for both a constant value of turbulent Schmidt number $Sc_t = 0.7$ and the proposed variable turbulent Schmidt number k_f–ε_f model are presented, showing the improved comparison to experimental data provided by the mixture-fraction variance model.

B. Supersonic Tangential Injection Mixing Layer

A nonreacting tangential flow experiment conducted by Burrows and Kurkov [28] is simulated using the mixture-faction variance k_f–ε_f model to predict mixing between a Mach 1.0 hydrogen stream at 254 K and a nitrogen/water-vapor stream flowing parallel at Mach 2.44, 1150 K, with a 0.767/0.233 mass ratio. The energy-variance model was used to predict turbulent thermal mixing between the streams. The experiment simulates a supersonic combustor arrangement, except that for the mixing study, an inert gas is used in the freestream. Application of the proposed models to a reacting case will be presented in the next section.

Model predictions for species mole fraction and total temperature are compared to experimental data measured at the exit plane of the combustor. Results are also presented using turbulent Prandtl and Schmidt numbers held constant at 0.5 and 0.9. Figure 9a shows the predicted species mole fractions at the exit plane compared to measured data, and suggests that $Sc_t = 0.9$ provides a good match to the exit plane data. The location $Y = 1.58$ cm corresponds to the coordinate at the top of the upstream injector. The result for $Sc_t = 0.5$ illustrates the sensitivity of the species mixing to the choice of turbulent Schmidt number.

Total temperature predictions vs measured data at the exit plane, normalized with wall and freestream temperatures, $\theta_t = (T_t - T_{t,w})/(T_{t,\infty} - T_{t,w})$, are provided in Fig. 9b. The energy-variance k_e–ε_e model captures the extent of the mixing region suggested by the data. The total temperature predictions are similar to those produced with a constant $Pr_t = 0.9$, except that there is slightly better agreement with the data closer to the wall using a variable Prandtl number. A constant $Pr_t = 0.5$ overpredicts the mixing.

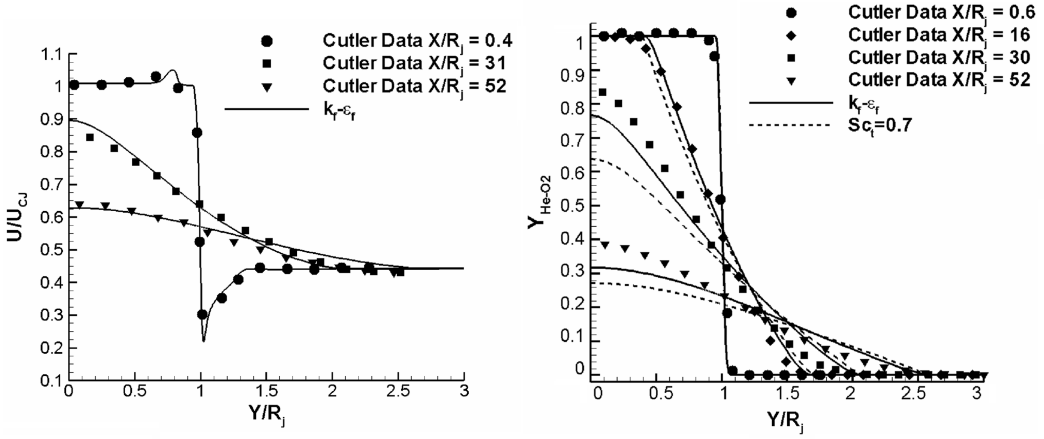

a) Jet velocity **b) Center jet mass fraction**

Fig. 8 Coflow helium–air jet predictions vs Cutler et al. [26,27] data.

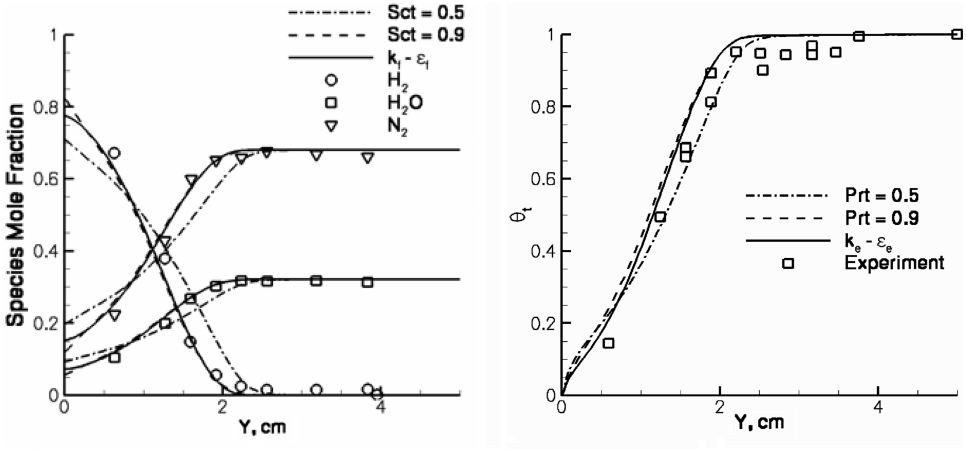

a) Species mole fraction b) Total temperature

Fig. 9 Burrows and Kurkov [28] mixing study exit plane predictions vs data.

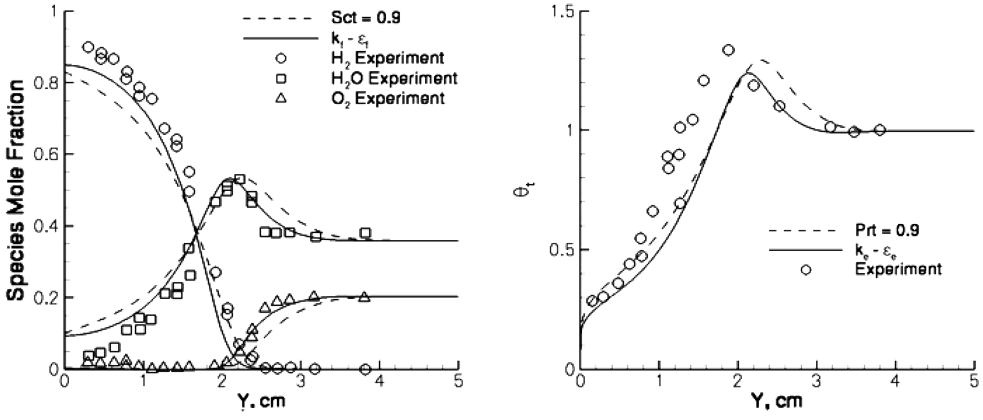

a) Species mole fraction b) Total temperature

Fig. 10 Burrows and Kurkov [28] combustion study exit plane predictions vs data.

V. Reacting Flow Studies

An aim of the current effort is to provide more accurate modeling of turbulence effects on energy and species mixing in high-speed combusting environments. As such, we have evaluated model performance for some basic high-speed reacting flows with comparison against experimental data. Recognizing that the combustion process involves added complexities, we restricted our attention to H_2/Air problems (where the kinetics is well established) under conditions for which burning should readily occur. Finite-rate chemistry was modeled using an abridged version of the 1988 Jachimowski mechanism [29], which excluded the reactions involving nitrogen. This mechanism contains 20 reactions and nine species (H, H_2, H_2O, O, O_2, OH, HO_2, H_2O_2, and N_2). It is found that the proposed scalar-variance models predict variations in turbulent Prandtl and Schmidt numbers that respond to the local reacting conditions and improve predictions over those achievable using constant values.

A. Supersonic Tangential Injection Combustor

The mixing layer experiment of Burrows and Kurkov [28] discussed in the preceding section was repeated with oxygen present in the freestream, to provide a combusting environment. A simulation using both the energy-variance and mixture-fraction variance models was performed. Total temperature, $\theta_t = (T_t - T_{t,w})/(T_{t,\infty} - T_{t,w})$, and species mole fraction predictions are compared with experimental data at the combustor exit plane in Fig. 10a and 10b. Results assuming constant values for turbulent Schmidt and Prandtl number are also presented. The comparisons show that use of the variance models provides a better match to the experimental data, because the turbulent Schmidt and Prandtl numbers can adjust to local conditions in the domain. Total temperature is somewhat underpredicted; however, the variable Prandtl number captures the return to freestream conditions better. Contours of predicted turbulent Prandtl and Schmidt number are shown in Fig. 11 just downstream of injector. The effect of the combustion on these parameters is evident as their behavior changes

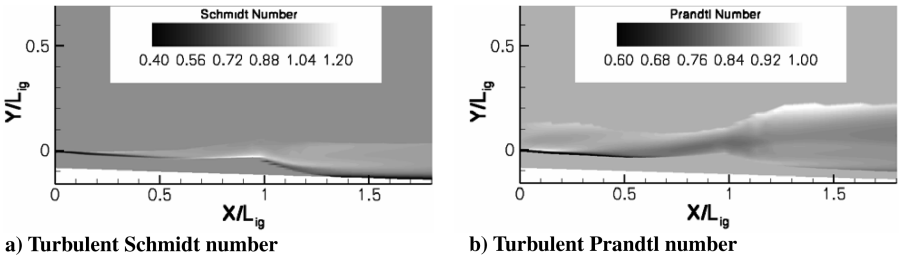

a) Turbulent Schmidt number b) Turbulent Prandtl number

Fig. 11 Burrows and Kurkov [28] combustion study; predicted values of turbulent Prandtl and Schmidt number.

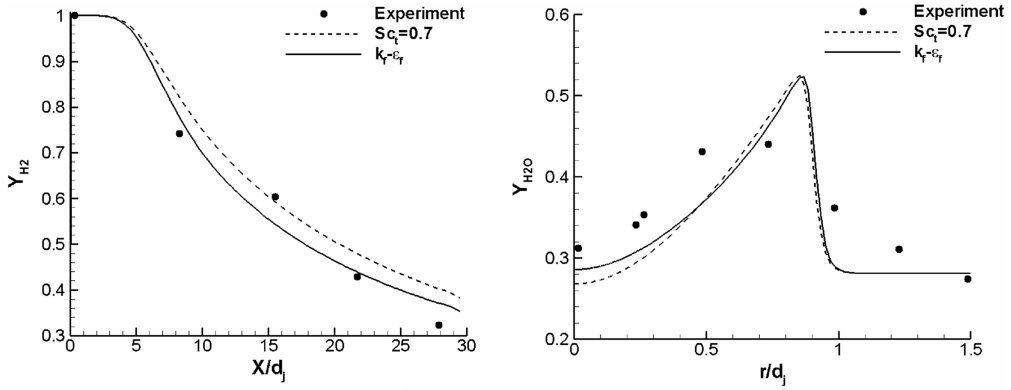

a) Centerline hydrogen mass fraction

b) Radial distribution of H_2O mass fraction at x/d_j=21.7

Fig. 12 Coxial beach jet predictions vs data.

significantly at the ignition point ($x/L_{\text{ig}} = 1$). Mild variations in both Pr_t and Sc_t occur within the shear layer upstream of the ignition point. At the ignition point, both profiles broaden due to heat release and flow dilatation, and Pr_t and Sc_t locally increase.

B. Supersonic Coaxial Jet

The Beach hydrogen/air coaxial reacting jet experiment documented by Evans et al. [30] was analyzed using the energy and mixture-fraction variance methodology. Results are compared with measured data. Predictions using constant values of turbulent Prandtl and Schmidt number, $Pr_t = Sc_t = 0.7$, typically suitable for a round jet, are also presented as a baseline calculation. The experiment consists of a Mach 2.0 hydrogen central jet discharging at a temperature of 251 K into a Mach 1.9 vitiated air freestream at a temperature of 1495 K. Jet nozzle turbulence conditions are specified based on comparisons to data for measured pressure at the jet exit and centerline nitrogen mass fraction. Figure 12a presents comparisons of hydrogen mass fraction along the jet centerline. Figure 12b presents comparisons of the radial distribution of water vapor mass fraction at an axial location of $x/d_j = 21.7$. The predictions compare well to the data, providing confirmation that the variable Sc_t and Pr_t formulations are capable of capturing the evolution of turbulent scalar transport within combusting flows. The predicted turbulent Prandtl and Schmidt number along the jet centerline are shown in Fig. 13, deviating from a constant value in the developing region of the jet, and then relaxing towards expected values further downstream. This capability of the scalar-variance methodology, to adjust Pr_t and Sc_t to local effects, allows for greater flexibility in modeling turbulent scalar mixing, particularly as more complex flows need to be considered where use of a single, constant valve for Pr_t and Sc_t is inadequate to capture the variation in turbulent scalar mixing.

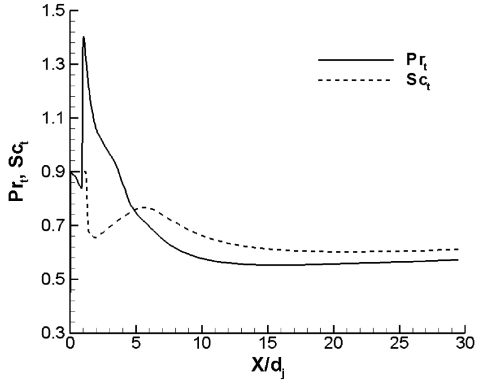

Fig. 13 Coaxial beach jet; centerline distribution of predicted turbulent Prandtl and Schmidt number.

VI. Conclusions

A scalar-variance model to predict variable turbulent Prandtl and Schmidt numbers has been formulated based on internal energy and mixture-fraction variance concepts. Transport equations for the scalar variance and its dissipation rate are presented. Turbulent Prandtl number is based on a ratio of the turbulent velocity time scale from a k–ε turbulence model to a thermal time scale based on the internal energy variance k_e and its dissipation rate ε_e. Turbulent Schmidt number for mass diffusivity is based on a ratio of the turbulent velocity time scale and a species-mixing time scale from a mixture-fraction variance k_f and its dissipation rate ε_f. The current formulation avoids higher-moment chemical source terms for reacting flows, which appear in alternate formulations and are difficult to accurately model. This enhancement makes the method attractive for combustion applications. Model predictions for a range of mixing and reacting flows with energy and/or species variance are compared with measured data. Significantly, the model constants are held fixed for the range of cases considered and good agreement to the experimental data is obtained without application-specific tuning of the constants. Compressibility effects for high-speed flows appear to be adequately modeled. The capability to predict and apply local values of turbulent Prandtl and Schmidt numbers for both mixing and reacting cases provides better computational agreement to experimental data than use of fixed Prandtl and Schmidt numbers. The scalar-variance models also provide information on fluctuating temperature and fluctuating species concentration, which are useful for a number of applications such as jet noise prediction and turbulence-chemistry interaction modeling.

Acknowledgment

Portions of this work have been supported under NASA, U.S. Air Force, and U.S. Army efforts.

References

[1] Sommer, T. P., So, R. M. C., and Zhang, H. S., "Near-Wall Variable-Prandlt Number Turbulence Model for Compressible Flows," *AIAA Journal*, Vol. 31, No. 1, 1993, pp. 27–35.

[2] Brinckman, K. W., Calhoon, W. H., Jr., Mattick, S., Tomes, J., and Dash, S. M., "Scalar Variance Model Validation for High-Speed Variable Composition Flows," AIAA Paper 2006-0715, Jan. 2006.

[3] Calhoon, W. H., Jr., Brinckman, K. W., Tomes, J., Mattick, S., and Dash, S. M., "Scalar Fluctuation and Transport Modeling for Application to High Speed Reacting Flows," AIAA Paper 2006-1452, Jan. 2006.

[4] Nagano, Y., and Kim. C., "A Two-Equation Model for Heat Transport in Wall Turbulent Shear Flows," *Journal of Heat Transfer*, Vol. 110, Aug. 1988, pp. 583–589.

[5] Nagano, Y., Tagawa, M., and Tsuji, T., "An Improved Two-Equation Heat Transfer Model for Wall Turbulent Shear Flows," *3rd ASME/JSME Thermal Engineering Conference Proceedings*, Vol. 3, American Society of Mechanical Engineers, New York, June 1991, pp. 233–240.

[6] Sommer, T. P., So, R. M. C., and Lai, Y. G., "A Near Wall Two-Equation Model for Turbulent Heat Fluxes," *International Journal of Heat and Mass Transfer*, Vol. 35, No. 12, 1992, pp. 3375–3387.
[7] Launder, B. E., "Heat and Mass Transport," *Turbulence—Topics in Applied Physics*, edited by P. Bradshaw, Springer, Berlin, 1976, pp. 232–287.
[8] Zhang, H. S., So, R. M. C., Speziale, C. G., and Lai, Y. G., "A Near-Wall Two-Equation Model for Compressible Turbulent Flows," *AIAA Journal*, Vol. 31, No. 1, 1993, pp. 196–199.
[9] Gerlinger, P., "Investigation of an Assumed PDF Approach for Finite-Rate Chemistry," AIAA Paper 2002-0166, Jan. 2002.
[10] Chidambaram, N., Dash, S. M., and Kenzakowski, D. C., "Scalar Variance Transport in the Turbulence Modeling of Propulsive Jets," *Journal of Propulsion and Power*, Vol. 17, No. 1, 2001, pp. 79–84.
[11] Calhoon, W. H., Jr., Kannepalli, C., Arunajatesan, S., and Dash, S. M., "Analysis of Scalar Fluctuations at High Convective Mach Numbers," AIAA Paper 2002-1087, Jan. 2002.
[12] Papp, J. L., and Dash, S. M., "Turbulence Model Unification and Assessment for High-Speed Aeropropulsive Flows," AIAA Paper 2001-0880, Jan. 2001.
[13] Nagano, Y., "Modeling Heat Transfer in Near-Wall Flows," *Closure Strategies for Turbulent and Transitional Flows*, edited by B. E. Launder and N. D. Sandham, Cambridge Press, Cambridge, England, 2002, pp. 188–247.
[14] Xiao, X., Edwards, J. R., Hassan, H. A., and Cutler, A. D., "Variable Turbulent Schmidt-Number Formulation for Scramjet Applications," *AIAA Journal*, Vol. 44, No. 3, March 2006, pp. 593–599.
[15] Xiao, X., Hassan, H. A., and Baurle, R. A., "Modeling Scramjet Flows with Variable Turbulent Prandtl and Schmidt Numbers," AIAA Paper 2006-0128, Jan. 2006.
[16] Launder, B. E., Morse, A., Rodi, W., and Spalding, D. B., "Prediction of Free Shear Flows, A Comparison of the Performance of Six Turbulence Models," *Free Turbulent Shear Flows—Conference Proceedings*, Vol. 1, NASA Langley Research Center, Hampton, VA, July 1972, pp. 361–426.
[17] Sarkar, S., "The Pressure-Dilation Correlation in Compressible Flows," *Physics of Fluids A*, Vol. 4, No. 12, Dec. 1992, pp. 2674–2682.
[18] Zeman, O., "Dilation Dissipation: The Concept and Application in Modeling Compressible Mixing Layers," *Physics of Fluids A*, Vol. 2, No. 2, Feb. 1990, pp. 178–188.
[19] Pope, S., "An Explanation of the Turbulent Round-Jet/Plane-Jet Anomaly," *AIAA Journal*, Vol. 16, No. 3, 1978, pp. 279–281.
[20] So, R. M. C., Sarkar, S., Gerodimos, G., and Zhang, J., "A Dissipation Rate Equation for Low-Reynolds-Number and Near-Wall Turbulence," *Theoretical and Computational Fluid Dynamics*, Vol. 9, No. 1, Aug. 1997, pp. 47–63.
[21] Abe, K., and Kondoh, T., "A New Turbulence Model for Predicting Fluid Flow and Heat Transfer in Separating and Reattaching Flows—2. Thermal Field Calculations," *International Journal of Heat and Mass Transfer*, Vol. 38, No. 8, 1995, pp. 1467–1481.
[22] Brinckman, K. W., Kenzakowski, D. C., and Dash, S. M., "Progress in Practical Scalar Fluctuation Modeling for High-Speed Aeropropulsive Flows," AIAA Paper 2005-0508, Jan. 2005.
[23] Lockwood, F. C., and Moneib, H. A., "Fluctuating Temperature Measurements in a Heated Round Free Jet," *Combustion Science and Technology*, Vol. 22, Nos. 1–2, 1980, pp. 63–81.
[24] Seiner, J. M., Ponton, M. K., Jansen, B. J., and Lagen, N. T., "The Effects of Temperature on Supersonic Jet Noise Emission," DGRL/AIAA Paper 92-02-046, May 1992.
[25] Erlebacher, G., Hussaini, M. Y., Speziale, C. C., and Zang, T. A., "Toward the Large-Eddy Simulation of Compressible Turbulent Flows," ICASE, Report No. 87-20, 1990.
[26] Cutler, A. D., Carty, A. A., Doerner, S. E., Diskin, G. S., and Drummond, J. P., "Supersonic Coaxial Jet Experiment for CFD Code Validation," AIAA Paper 99-3588,June–July 1999.
[27] Cutler, A. D., Diskin, G. S., Danehy, P. M., and Drummond, J. P., "Fundamental Mixing and Combustion Experiments for Propelled Hypersonic Flight," AIAA Paper 2002-3879, July 2002.
[28] Burrows, M. C., and Kurkov, A. P., "Analytical and Experimental Study of Supersonic Combustion of Hydrogen in a Vitiated Airstream," NASA Technical Memorandum TM X-2828, Sept. 1973.
[29] Jachimowski, C. J., "An Analytical Study of the Hydrogen-Air Reaction Mechanism with Application to Scramjet Combustion," NASA TP 2791, 1988.
[30] Evans, J. S., Schexnayder, J., Jr., and Beach, H. L., Jr., "Application of a Two-Dimensional Parabolic Computer Program to Prediction of Turbulent Reacting Flows," NASA TP1169, March 1978.

D. Gaitonde
Associate Editor